



**HAL**  
open science

# The curvature elasticity of fluid membranes: A catalogue of vesicle shapes

H.J. Deuling, W. Helfrich

► **To cite this version:**

H.J. Deuling, W. Helfrich. The curvature elasticity of fluid membranes: A catalogue of vesicle shapes. *Journal de Physique*, 1976, 37 (11), pp.1335-1345. 10.1051/jphys:0197600370110133500 . jpa-00208531

**HAL Id: jpa-00208531**

**<https://hal.science/jpa-00208531>**

Submitted on 4 Feb 2008

**HAL** is a multi-disciplinary open access archive for the deposit and dissemination of scientific research documents, whether they are published or not. The documents may come from teaching and research institutions in France or abroad, or from public or private research centers.

L'archive ouverte pluridisciplinaire **HAL**, est destinée au dépôt et à la diffusion de documents scientifiques de niveau recherche, publiés ou non, émanant des établissements d'enseignement et de recherche français ou étrangers, des laboratoires publics ou privés.

Classification  
*Physics Abstracts*  
 7.130

## THE CURVATURE ELASTICITY OF FLUID MEMBRANES : A CATALOGUE OF VESICLE SHAPES

H. J. DEULING and W. HELFRICH

Institut fuer Theoretische Physik  
 Freie Universität Berlin, D 1 Berlin-33, Arnimallee 3, Germany

(Reçu le 21 mai 1976, accepté le 15 juin 1976)

**Résumé.** — Les formes des membranes fermées fluides formées par la lécithine dans l'eau ont été calculées en fonction du volume délimité, de la surface de la membrane, et de la courbure spontanée. Diverses formes symétriques par rotation sont présentées avec des indentations, des cavités et des surfaces de contact.

**Abstract.** — Shapes of closed fluid membranes such as those formed by lecithin in water were calculated as a function of enclosed volume, membrane area and spontaneous curvature. As the area can be taken to be constant, the only elasticity controlling the shapes of these vesicles is that of curvature. A large variety of rotationally symmetric shapes are presented, allowing for indentations, cavities and contact of the membrane with itself.

1. **Introduction.** — Lipid bilayer membranes have been the subject of many investigations over the last decade, because they seem to be closely related to biological membranes. They are composed of a double layer of lipid molecules. The hydrophilic heads of the molecules are pointing towards the aqueous medium and the hydrophobic ends of the hydrocarbon chains are pointing towards the interior of the film. Lipid bilayers can be prepared in such a way that the membranes close to form vesicles whose diameters can range from a few hundred Å [1] to several mm [2]. The shape of such vesicles is controlled by the elastic properties of the lipid bilayer. Provided that the membrane is fluid and the vesicle does not form a sphere, the only important elasticity is that of curvature [3].

In the following, the lipid bilayer membrane is always assumed to be a two-dimensional fluid characterized by a vanishing modulus of shear elasticity. Area dilation of the membrane is negligible, except for spherical vesicles under excess internal pressure, as much more energy is required for area dilation than for curvature. Practically all the deformational energy of a vesicle is therefore stored in the curvature (or bending) of the membrane. On the basis of Hooke's law one should expect the curvature energy per unit area of the lipid bilayer to be proportional to the curvature squared. Such an ansatz would imply that the plane bilayer is the equilibrium state in the absence of external forces. A lipid bilayer may, however, possess a built-in asymmetry due to either a different lipid composition of the two constituent monolayers

or different environments on the two sides of the bilayer. Then the membrane has non-zero curvature in its state of lowest elastic energy. Allowing for such a *spontaneous curvature*, we may write for the bending energy per unit area [3]

$$g_c = (1/2) k_c (c_1 + c_2 - c_0)^2 + (1/2) \bar{k}_c c_1 c_2 \quad (1.1)$$

where  $k_c$  and  $\bar{k}_c$  are elastic constants and  $c_1$  and  $c_2$  are the two principal curvatures. The phenomenological parameter  $c_0$  is the spontaneous curvature. If the constituent monolayers are free to slide over each other, as is generally assumed,  $c_0$  is constant over the entire area of a vesicle. It may be noted that for actual shape changes  $c_0$  may be a time-dependent functional of the deformation [4]. The concept of curvature elasticity, including spontaneous curvature, has recently been applied to red blood cells [5] to explain the biconcave discoid shape of erythrocytes. Analyzing the experimental data of Evans and Fung [6], the present authors [7] found  $c_0 = -0.74 \mu\text{m}^{-1}$  for the membrane of normal human erythrocytes under physiological conditions. (The minus sign indicates a spontaneous curvature opposite to that of the sphere.) In the present paper we use the concept of curvature elasticity to calculate theoretical shapes of lipid bilayer vesicles and classify the most important solutions of rotational symmetry. We also calculate the dependence of vesicle volume on the difference in osmotic pressures inside and outside the vesicle as well as the relation between the total curvature energy and volume for the different types of shapes. To

designate vesicle shapes, particularly the more exotic ones, we will often use the nomenclature developed for red blood cells [8]. In all cases examples of the shapes are shown in the figures.

**2. Theory.** — Expression (1.1) for the bending energy per unit area of a lipid bilayer membrane is closely analogous to that for the energy density of a liquid crystal [9], the first term in (1.1) corresponding to the splay term of liquid crystals and the second term being analogous to the saddle splay term [10]. This second term, when integrated over the surface of a vesicle, gives a contribution to the total curvature energy which is independent of the shape according to Gauss' theorem. Consequently, the shape of the vesicle is determined only by the first term in expression (1.1). For a vesicle with surface area  $S$  we define an equivalent sphere radius  $R_0$  by  $S = 4 \pi R_0^2$ . The maximal volume of the vesicle at constant surface area  $S$  is  $V_0 = (4 \pi/3) R_0^3$ . When the volume  $V$  is reduced below  $V_0$ , the vesicle becomes easily deformable and can assume a large variety of shapes depending on  $S$ ,  $V$ , and  $c_0$ . To find the equilibrium shape of a vesicle, we have to look for minima of the total curvature elastic energy  $E = \int g_c dS$  at constant surface area and constant volume. We introduce Lagrange multipliers  $\Delta p$  and  $\lambda$  for the constraints  $V = \text{const.}$  and  $S = \text{const.}$ , respectively.  $\Delta p = p_e - p_i$  represents the osmotic pressure difference between the outer and inner medium and  $\lambda$  represents a tensile stress. The shape of the vesicle at equilibrium is found from the equation

$$\delta \left\{ (1/2) k_c \int (c_1 + c_2 - c_0)^2 dS + \Delta p V + \lambda S \right\} = 0 \quad (2.1)$$

To keep the problem simple, we consider only forms having rotational symmetry. The principal curvatures in this case are those along the meridians ( $c_m$ ) and along the parallels of latitude ( $c_p$ ). We describe the contour of the cell by a function  $z(x)$ , the  $z$ -axis coinciding with, and  $x$  being the distance from, the axis of rotation. Denoting by  $\psi$  the angle made by the surface normal and the  $z$ -axis, we can express the curvatures  $c_m$  and  $c_p$  by  $\psi(x)$

$$c_p = \frac{\sin \psi(x)}{x}, \quad c_m = \cos \psi(x) \frac{d\psi}{dx}. \quad (2.2)$$

The angle  $\psi(x)$  in turn is related to the contour  $z(x)$  by

$$\frac{dz}{dx} = - \tan \psi(x). \quad (2.3)$$

Eliminating  $\psi(x)$ , we obtain a differential equation expressing the assumption of rotational symmetry

$$\frac{dc_p}{dx} = \frac{c_m - c_p}{x}. \quad (2.4)$$

We express the contour  $z(x)$  and volume and surface area in terms of  $x$  and  $c_p$

$$z(x) = z(0) - \int x c_p [1 - (x c_p)^2]^{-1/2} dx \quad (2.5)$$

$$dV = \pi x^3 c_p [1 - (x c_p)^2]^{-1/2} dx \quad (2.6)$$

$$dS = 2 \pi x [1 - (x c_p)^2]^{-1/2} dx. \quad (2.7)$$

When using expressions (2.6) and (2.7) we have to take into account that  $z(x)$  is double valued. We have to integrate over  $x$  from 0 to the maximal value  $x_m$  and back to zero to obtain the total volume and surface area, respectively. With the aid of expressions (2.4), (2.6) and (2.7) we can rewrite the variational problem in the following form

$$\delta \int_0^{x_m} x [1 - (x c_p)^2]^{-1/2} \left\{ \left( x \frac{dc_p}{dx} + 2 c_p - c_0 \right)^2 + (\Delta p/k_c) x^2 c_p + 2(\lambda/k_c) \right\} dx = 0. \quad (2.8)$$

The Euler-Lagrange equation corresponding to this variational problem reads

$$\frac{dc_m}{dx} = x [1 - (x c_p)^2]^{-1} \left\{ (1/2) c_p [(c_p - c_0)^2 - c_m^2] + (\lambda/k_c) c_p + (1/2) (\Delta p/k_c) \right\} - (c_m - c_p)/x. \quad (2.9)$$

The two non-linear differential equations (2.4) and (2.9) can be solved numerically [5]. From the solution  $c_p(x)$ , the contour  $z(x)$  is obtainable by a further integration using expression (2.5). The boundary conditions for the equations (2.4) and (2.9) can be discussed more easily when a slightly different formulation is used. We replace the independent variable  $x$  by the normalized surface area  $s$  using the relation

$$dx = \pm (2/x) [1 - (x c_p)^2]^{1/2} ds. \quad (2.10)$$

The variable  $s$  ranges from  $s = 0$  at the upper pole to a value  $s_m$  at the dividing parallel of latitude and from there to  $s = 1$  at the lower pole.  $dx/ds$  is positive in the upper half and negative in the lower half. We also use  $f = x^2$  instead of  $x$ . With these substitutions we obtain a system of three non-linear equations for the three dependent variables  $c_m(s)$ ,  $c_p(s)$  and  $f(s)$

$$\frac{dc_m}{ds} = \pm (1 - f c_p^2)^{-1/2} \times \left\{ c_p [(c_p - c_0)^2 - c_m^2] + 2(\lambda/k_c) c_p + (\Delta p/k_c) - 2(1 - f c_p^2) (c_m - c_p)/f \right\} \quad (2.11)$$

$$\frac{dc_p}{ds} = \pm 2(1 - f c_p^2)^{1/2} (c_m - c_p)/f \quad (2.12)$$

$$\frac{df}{ds} = \pm 4(1 - f c_p^2)^{1/2}. \quad (2.13)$$

These equations have different classes of solutions which are characterized by different boundary conditions which we shall discuss in detail below.

From the solution  $f(s)$ ,  $c_p(s)$ ,  $c_m(s)$  we find the volume  $V$  and the contour  $z(s)$  by further integrations

$$V/V_0 = (3/2) \int_0^1 f(s) c_p(s) ds \quad (2.14)$$

$$z(s) = z(0) - 2 \int c_p(s) ds. \quad (2.15)$$

For weak deformations of a sphere, i.e.  $V \approx V_0$ , there exist two solutions of equations (2.11)-(2.13) representing an elongated ellipsoid of revolution and an oblate ellipsoid of revolution, respectively. The value of  $c_0$  determines which of the two shapes has lower elastic energy. When  $c_0$  is below a critical value  $c_{0c}$ , the oblate shape has lower energy than the prolate form. If however  $c_0$  is greater than  $c_{0c}$  the elongated ellipsoid of revolution represents the stable form. The critical spontaneous curvature  $c_{0c}$  was found to be  $c_{0c} = -(39/23) R_0^{-1}$ . The derivation is given in appendix B. As the volume is increased to the maximal value  $V_0$ , the osmotic pressure difference  $\Delta p$  between the inside and the outside of the ellipsoids attains the value [3]  $\Delta p_c = (12 - 2 c_0 R_0) k_c R_0^{-3}$ . In the following we will always give  $\Delta p$  in units of  $\Delta p_c$ .

**3. Numerical results and discussion.** — The differential equations derived in section 2 have a singularity wherever either  $f(s)$  goes to zero or  $f(s) c_p^2(s)$  approaches 1. We can remove these singularities by choosing correct boundary conditions. At the poles of the vesicle, i.e. at  $s = 0$  and  $s = 1$ , we have  $f = 0$ . As we approach the poles, however, the difference  $c_m - c_p$  also goes to zero. We can therefore take the correct limit of equation (2.12) and obtain

$$\left. \frac{dc_p}{ds} \right|_{s=0} = (1/3) \left. \frac{dc_m}{ds} \right|_{s=0} \quad (3.1)$$

Whenever  $f(s)$  reaches an extremum at some point  $s = s_m$  the quantity  $f(s) c_p^2(s)$  becomes equal to 1 and equation (2.11) has a singularity. We can remove this singularity by the boundary condition that at  $s = s_m$  the expression in curly brackets in equation (2.11) also vanishes. This defines either the Lagrangian multiplier  $\lambda$  or the curvature  $c_m(s)$  at  $s = s_m$ :

$$\lambda/k_c = -(\Delta p/k_c)/2 - c_p(s_m) \times [(c_p(s_m) - c_0)^2 - c_m^2(s_m)]. \quad (3.2)$$

Taking the correct limit  $s \rightarrow s_m$  of equation (2.11) we find the equation to be consistent with any value of  $\gamma = (dc_m/ds)_{s=s_m}$ . The second derivatives are all well defined at  $s = s_m$ . Therefore we make a Taylor expansion around the point  $s = s_m$  at which equa-

tion (2.11) is ill-defined :

$$\begin{aligned} c_m(s) &= c_m(s_m) + \gamma(s - s_m) + \\ &+ (1/2) \left. \frac{d^2 c_m}{ds^2} \right|_{s=s_m} (s - s_m)^2 + \dots \\ c_p(s) &= c_p(s_m) + \\ &+ (1/2) \left. \frac{d^2 c_p}{ds^2} \right|_{s=s_m} (s - s_m)^2 + \dots \quad (3.3) \\ f(s) &= f(s_m) + \\ &+ (1/2) \left. \frac{d^2 f}{ds^2} \right|_{s=s_m} (s - s_m)^2 + \dots \end{aligned}$$

Besides rotational symmetry, ellipsoids of revolution and disk-shaped cells (discocytes) also possess reflection symmetry with respect to the equatorial plane. Dealing with these forms we have only to consider the interval  $0 \leq s \leq 0.5$ . At  $s = 0$  we have  $f = 0$  and  $c_m = c_p = c_m^0$ . At  $s = 0.5$  we have  $f = f_m$ ,  $c_p = f_m^{-1/2}$  and  $c_m = c_m^m$ . The parameter  $\gamma$  is zero because the solution is symmetric with respect to the point  $s = 0.5$ . We start the solution at  $s = 0$  and at  $s = 0.5$  and match the branches at  $s = 0.25$  or at some other intermediate point. The matching condition for the three functions  $c_m(s)$ ,  $c_p(s)$  and  $f(s)$  gives three non-linear equations for the unknown boundary conditions  $c_m^0$ ,  $f_m$  and  $c_m^m$ . These three non-linear equations which we solve by the Newton-Raphson method [11] may have several solutions as we shall see below. Figure 1 shows such a solution for  $V/V_0 = 0.75$  and  $c_0 R_0 = -2.0$ . The contour of the cell corresponding to this solution is found by a further integration. It is shown in figure 3a. This type of cell is called discocyte. The scheme outlined above serves to find solutions for a given value of  $\Delta p/\Delta p_c$ . To calculate a cell-shape for a given volume  $V/V_0$  we treat  $\Delta p$  as an additional variable which is to be determined by equation (2.14).

When there is no reflection symmetry we have to solve the equations in the entire interval  $0 \leq s \leq 1$ . At  $s = 0$  we again have  $c_m = c_p = c_m^0$  and at  $s = 1$

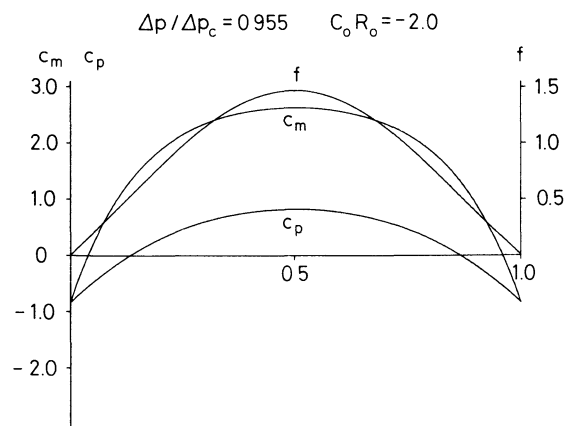


FIG. 1. — Plot of  $f(s)$ ,  $c_m(s)$  and  $c_p(s)$  versus  $s$  for a discocyte with  $V/V_0 = 0.75$  and  $c_0 R_0 = -2.0$ . The curvatures are given in units of  $R_0^{-1}$ ,  $f(s)$  is given in units of  $R_0^2$ .

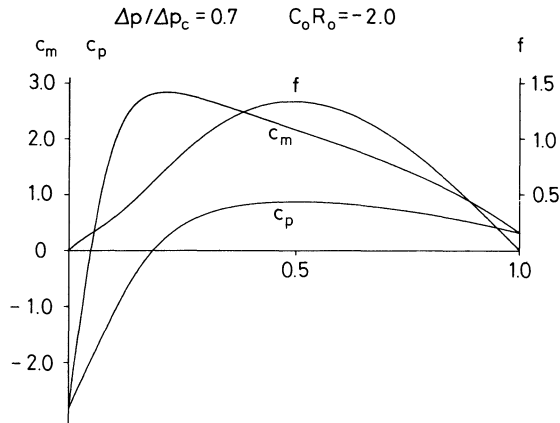


FIG. 2. — Plot of  $f(s)$ ,  $c_m(s)$  and  $c_p(s)$  versus  $s$  for a cup-shaped cell with  $V/V_0 = 0.75$  and  $c_0 R_0 = -2.0$ .

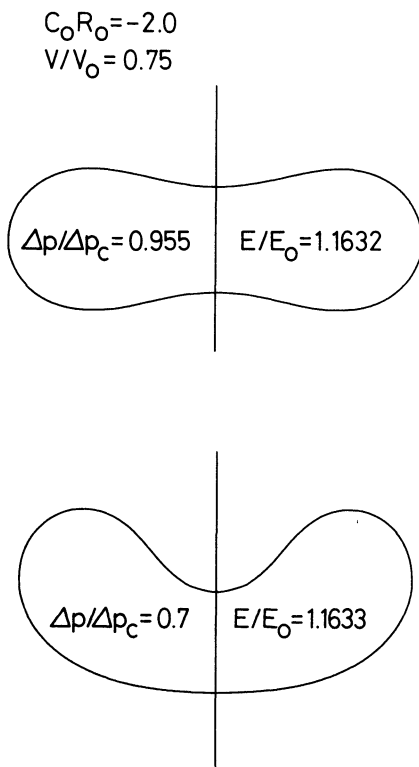


FIG. 3. — Contours corresponding to the solutions shown in figure 1a and figure 2b.

$c_m = c_p = c_m^1$ , the superscripts u and l referring to the upper and lower half of the cell respectively.  $c_m^u$  and  $c_m^l$  are unknown and still to be determined by boundary conditions. The function  $f(s)$  reaches its maximum  $f_m$  at some point  $s = s_m$ . At this point  $c_m(s)$  has some value  $c_m^m$ . The parameter  $\gamma$  is now different from zero. So we have to determine six unknown parameters  $c_m^u$ ,  $c_m^l$ ,  $c_m^m$ ,  $f_m$ ,  $\gamma$ ,  $s_m$ . Matching of the functions  $c_m(s)$ ,  $c_p(s)$  and  $f(s)$  at two intermediate points in the intervals  $0 \leq s \leq s_m$  and  $s_m \leq s \leq 1$  gives us six non-linear equations for the six unknown boundary conditions. These non-linear equations have more than one solution as we shall see below.

We calculate the solutions using again the Newton-Raphson method. Figure 2 shows the solution for  $V/V_0 = 0.75$  and  $c_0 R_0 = -2.0$ . The contour corresponding to this solution is shown in figure 3b. This type of vesicle is called a cup-shaped cell. Both solutions correspond to minima in the deformational energy, as is discussed in detail in appendix A.

As pointed out above, the non-linear equations for the boundary values have several solutions. In figure 4 we show two other symmetrical solutions representing higher order deformations of the sphere (only one quadrant is shown). Figure 5 shows a higher order asymmetric solution assuming a bell-shaped form when the volume is decreased further. Figure 6 and figure 7 show two other higher order deformations of the sphere. We have not investigated the stability of these forms.

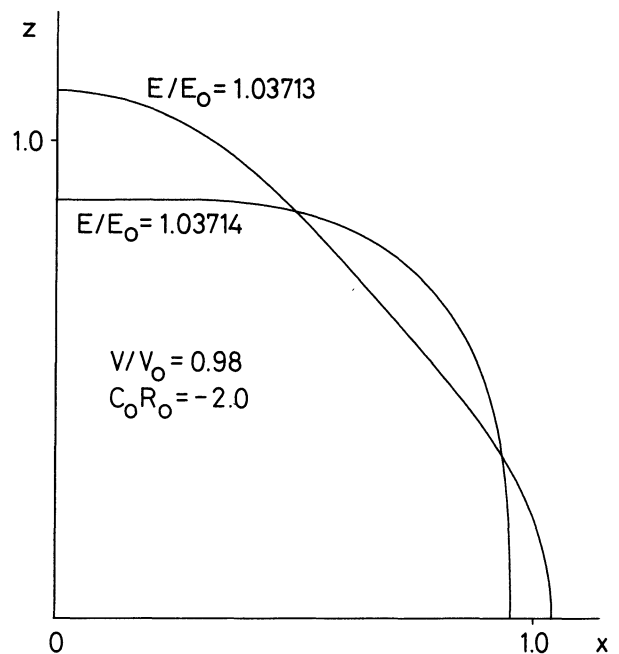


FIG. 4. — Contours of two symmetric solutions of higher order (only one quadrant is shown, the rotational axis is along  $z$ ).

When the volume is sufficiently reduced and the spontaneous curvature is not too small, the two halves of the symmetric discocyte (Fig. 3a) touch at the center. They are in contact over a circular area of radius  $x_0 = f_0^{1/2}$  and area  $f_0/4$  (in units of  $4 \pi R_0^2$ ). In the range  $0 \leq s \leq f_0/4$  we have  $c_m(s) = c_p(s) = 0$ . At  $s = f_0/4$ ,  $c_m(s)$  changes discontinuously to some value  $c_m^0$ . The discontinuity corresponds to a normal force per unit length along the circle bounding the area of contact. The force in the upper half of the cell is balanced by an opposite force per unit length at  $s = 1 - f_0/4$  in the lower half. At  $s = 0.5$  we have the same conditions as for discocytes. Now we have four unknown boundary values  $f_0$ ,  $c_m^0$ ,  $f_m$ ,  $c_m^m$ . The matching conditions give three equations as before and a fourth equation is obtained by the condition of contact  $z(s = f_0/4) = z(s = 0.5) = 0$ . The four

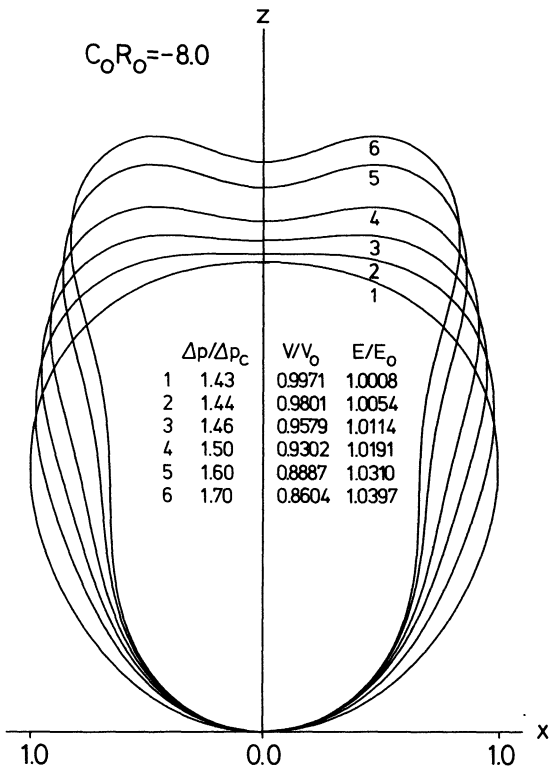


FIG. 5. — Contours of asymmetric solutions which are characterized by an almost triangular cross-section.

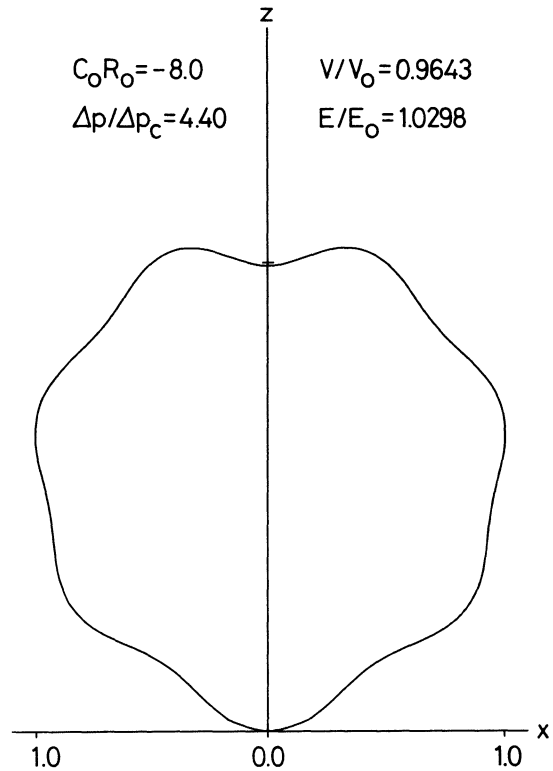


FIG. 7. — Contour of an asymmetric solution of higher order having heptagonal shape.

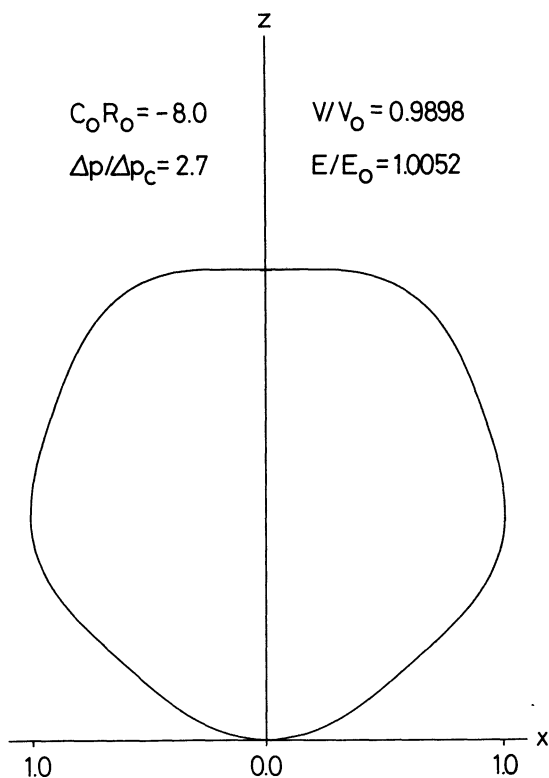


FIG. 6. — Contour of an asymmetric solution of higher order having pentagonal shape.

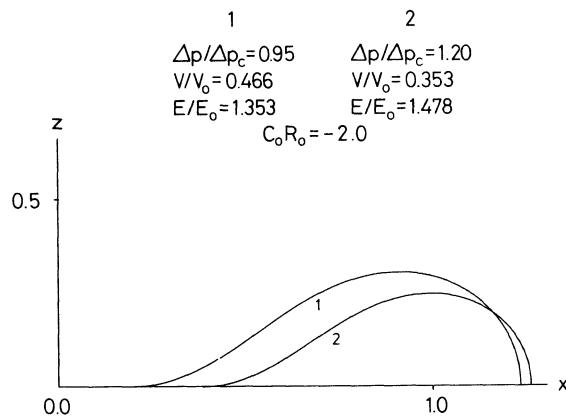


FIG. 8. — Two contours of torocytes (only one quadrant is shown, the rotational axis is along the z direction).

equations are solved by the Newton-Raphson method. Contours of two such torocytes are shown in figure 8. In calculating the torocytes we have neglected the

cohesive energy between the membrane regions which are in contact.

For the three types of solutions discussed so far we have calculated the dependence of volume  $V$  on osmotic pressure difference  $\Delta p$  for certain values of spontaneous curvature. Such a plot is shown in figure 9 for  $c_0 R_0 = -2.0$ . The asymmetric branch of solutions representing cup-shaped cells (see Fig. 3b) meets the symmetric branch of discocytes at a point marked by a critical pressure difference  $\Delta p_t$  and a critical volume  $V_t$ . No asymmetric solutions exist for  $\Delta p > \Delta p_t$  and  $V < V_t$ . The occurrence of such a threshold in the volume versus pressure diagram is a consequence of breaking reflection symmetry in going

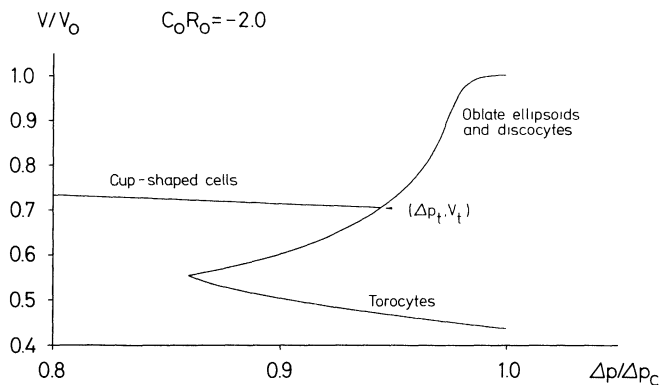


FIG. 9. — Plot of volume  $V$  (in units of  $V_0$ ) versus pressure difference  $\Delta p$  (in units of  $\Delta p_c$ ) for discocytes, cup-shaped cells and torocytes calculated for  $c_0 R_0 = -2.0$ .

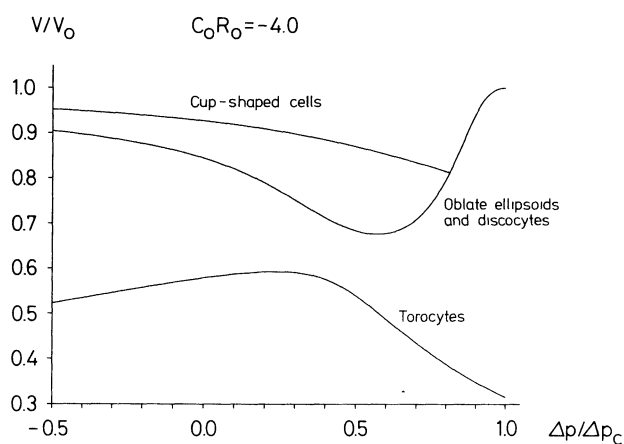


FIG. 10. — Plot of volume  $V$  versus pressure difference  $\Delta p$  calculated for  $c_0 R_0 = -4.0$ . A *volume gap* appears between the torocyte and the discocyte branch.

from the discocyte to the cup-shaped cell. Figure 10 shows the same diagram calculated for  $c_0 R_0 = -4.0$ . The discocyte and torocyte branches are no longer connected. With decreasing pressure difference  $\Delta p$ , the volume of the discocytes decreases at first and then increases again after having passed through a minimum. For a given volume we therefore find two symmetric solutions as is shown in figure 11 for

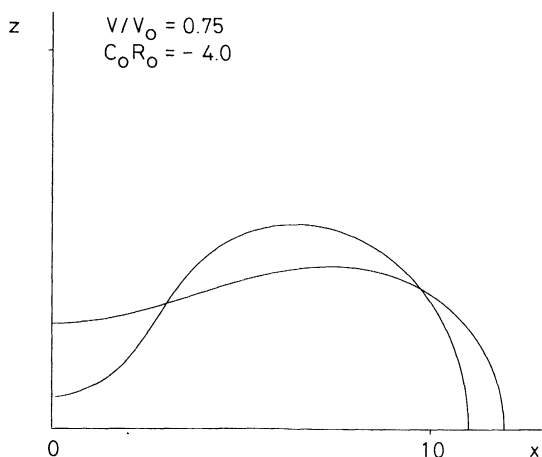


FIG. 11. — Two discocytes of volume  $V/V_0 = 0.75$ . These solutions differ in their values for  $\Delta p/\Delta p_c$ .

$V/V_0 = 0.75$ . The volume of the torocytes increases first with decreasing  $\Delta p$  and decreases again after passing through a maximum. Between this maximum volume for torocytes and the minimum volume for discocytes there is a *volume gap* where neither torocytes nor discocytes exist (but other rotationally symmetric forms may, of course, exist). If we had, for example, a discocyte with  $V/V_0 = 0.65$  and  $c_0 R_0 = -2.0$  and then by some chemical means decreased the spontaneous curvature  $c_0$ , we would reach a point where the vesicle could no longer have a biconcave-discoid shape but would undergo a sudden transition to a new equilibrium shape which might no longer have rotational symmetry. We can construct such a solution, if we compare the cup-shaped cell and the discocyte for  $\Delta p = -0.5 \Delta p_c$ , which are shown in figure 12. Both forms are nearly spherical.

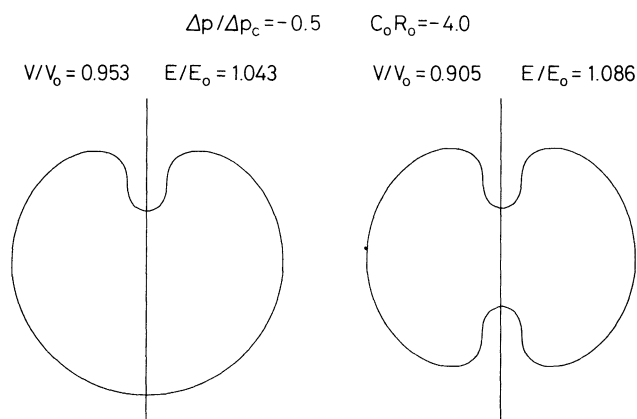


FIG. 12. — Contours of a cup-shaped cell and a discocyte for which the deviations from the spherical shape have become very localized.

The deviations from the sphere having become very localized at the poles we obtain spheres with *defects*. We find an energy  $E = 0.043 E_0$  and a volume decrease  $\Delta V = -0.047 V_0$  per defect for the shape of figure 12. Placing a number of such defects on a sphere in a regular or almost regular pattern, we obtain non-rotationally symmetric solutions, which are called *inverted echinocytes*. Another possible solution could be a form where the spikes point to the outside of the sphere rather than to the inside, which would be called an *echinocyte*. However, we cannot prove at present that the vesicle will assume either of these forms. From the numerical results shown in figure 10 we can only conclude that the discocyte becomes unstable when  $c_0$  is made sufficiently negative.

Instead of oblate ellipsoids and discocytes which we found for  $\Delta p < \Delta p_c$ , we can obtain prolate ellipsoids, if we choose  $\Delta p > \Delta p_c$ . (This holds only for  $c_0 < c_{0c}$ . For  $c_0 > c_{0c}$  we find oblate ellipsoids above  $\Delta p_c$  and prolate ellipsoids below  $\Delta p_c$ .) For these forms we have  $c_m(s) \leq c_p(s)$ . As we reduce the volume, the curvature at the dividing parallel of latitude  $c_m(0.5)$  quickly goes to zero. If we reduce the volume

further, we get dumbbell-shaped vesicles, as shown in figure 13. The calculation for dumbbells is complicated by the fact that we now have an additional singularity. The function  $f(s)$  has a minimum  $f_0$  at  $s = 0.5$  and a maximum  $f_m$  at some value  $s = s_m$ . At  $s = 0.5$  we have the initial conditions  $f = f_0$ ,  $c_p = f_0^{-1/2}$ ,  $c_m = c_m^m$ .

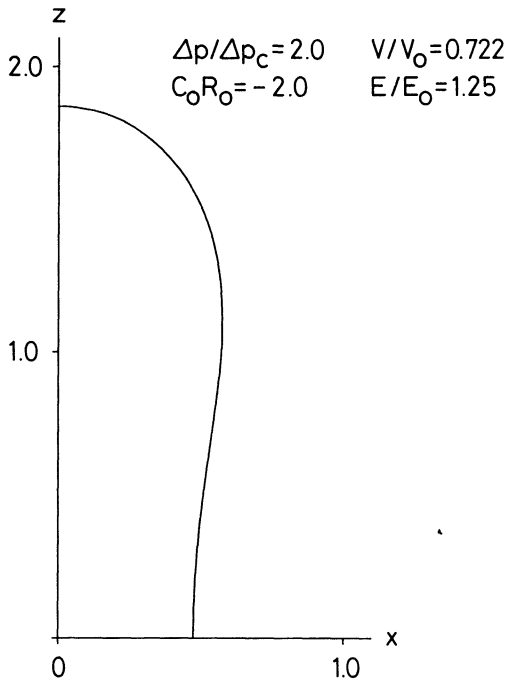


FIG. 13. — Contour of a dumbbell (only one quadrant is shown).

The parameter  $\lambda$  is now found from equation (3.2) and the solution is started with the expansion (3.3), where we have to put  $\gamma = 0$ , since the form is symmetric with respect to the equatorial plane. At  $s = s_m$  we have the initial condition  $f = f_m$ ,  $c_p = f_m^{-1/2}$ . The initial value for  $c_m(s)$  at  $s = s_m$  is now found from equation (3.2), since  $\lambda$  has been determined at  $s = 0.5$ . We start the solution again at  $s = s_m$  by using the expansion (3.3), where we now have to allow for a linear term with  $\gamma \neq 0$ . At  $s = 0$  we have the initial condition  $c_p = c_m = c_m^0$ . The six unknown parameters  $c_m^0$ ,  $c_m^m$ ,  $f_0$ ,  $f_m$ ,  $s_m$ ,  $\gamma$  have to be determined by matching the three functions  $f(s)$ ,  $c_p(s)$  and  $c_m(s)$  at two intermediate points in the intervals  $0 \leq s \leq s_m$  and  $s_m \leq s \leq 0.5$ . The calculation becomes inaccurate in the vicinity of the point where the vesicle goes from the dumbbell-shape to the ellipsoidal form, since at this point we would have to go to fourth order in the expansion (3.3) at  $s = 0.5$  and at  $s = s_m$ . In figure 14 we show the dependence of volume on pressure difference  $\Delta p$  for  $c_0 R_0 = -2.0$  and  $c_0 R_0 = -4.0$ . The branches for ellipsoids and for dumbbells do not join smoothly because of the inaccuracy of our calculation mentioned above. In figure 15 we give the dependence of the total deformational energy  $E$  on volume  $V$ . The energy is given in units of

$$E_0 = 2 \pi k_c (2 - c_0 R_0)^2,$$

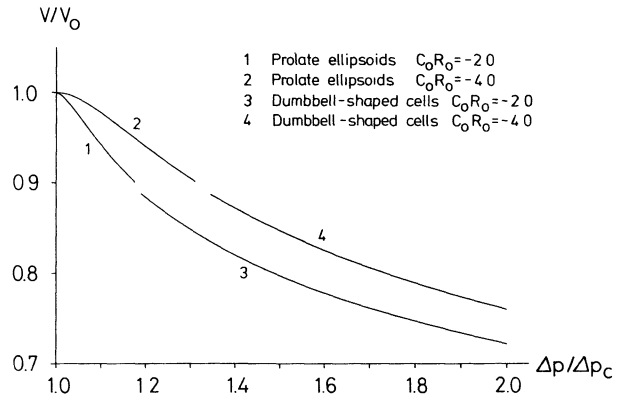


FIG. 14. — Plot of volume versus pressure difference for prolate ellipsoids and dumbbells.

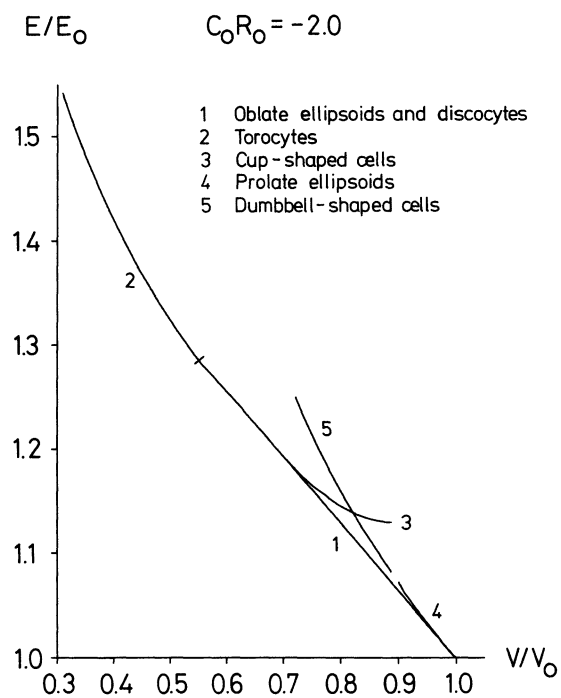


FIG. 15. — Plot of the deformational energy  $E$  (in units of the energy of a sphere  $E_0$ ) versus volume  $V$  (in units of  $V_0$ ) calculated for various forms with  $c_0 R_0 = -2.0$ .

which is the energy of a sphere. The results in figure 15 calculated for  $c_0 R_0 = -2.0$  show the energy of the cup-shaped cells to be higher than the energy of discocytes having the same volume. The sign of the energy difference is independent of the magnitude of  $c_0$ .

As pointed out above, cup-shaped cells exist only above a critical volume  $V_t$ . The magnitude of  $V_t$  decreases with increasing  $c_0$ . Choosing  $c_0$  to be zero or slightly positive, we can obtain cup-shaped cells which are very thin at the center. Such a form is shown in figure 16 for  $c_0 R_0 = 0$ . Increasing  $c_0$  and at the same time decreasing the volume, we can cause the two halves of the cell membrane to make contact over some area at the center. Such a cell is shown in figure 17 and referred to in the following as codocyte I.

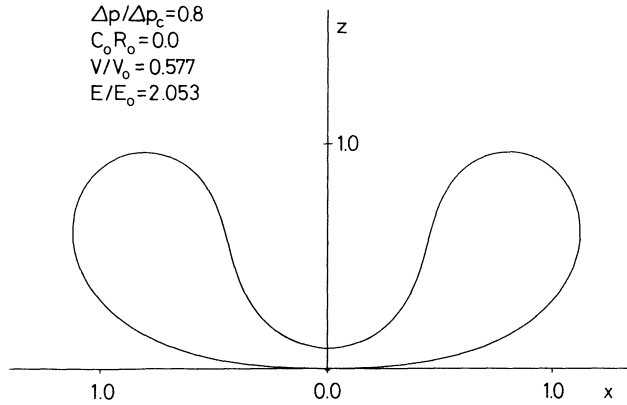


FIG. 16. — Contour of a deep cup-shaped cell.

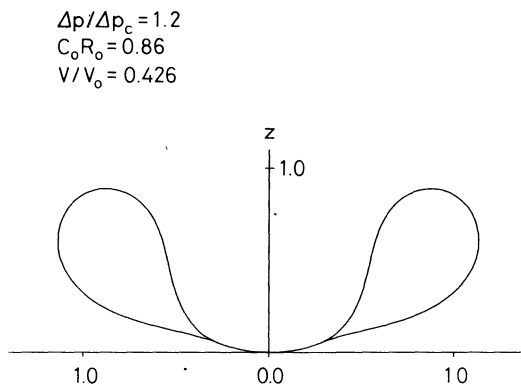


FIG. 17. — Contour of a codocyte I.

We calculate this type of solution using the following boundary conditions. In the range of  $0 \leq s < s_0$  and  $1 - s_0 < s \leq 1$  the two membrane halves are in contact and the curvatures are  $c_m(s) = c_p(s) = \text{const}$ . At the points  $s = s_0$  and  $s = 1 - s_0$  the curvature  $c_p(s)$  is continuous, whereas  $c_m(s)$  changes discontinuously to a value  $c_m^u$  at  $s = s_0$  and to  $c_m^l$  at  $s = 1 - s_0$ . The discontinuities in  $c_m(s)$  at  $s = s_0$  and  $s = 1 - s_0$  respectively correspond to normal forces per unit length along the circle bounding the area of contact. Since the contributions of the upper and lower halves must balance each other, we have

$$c_m(s) = c_p(s) = (1/2) (c_m^u - c_m^l)$$

in the range  $0 \leq s < s_0$  and

$$c_m(s) = c_p(s) = - (1/2) (c_m^u - c_m^l)$$

in the range  $1 - s_0 < s \leq 1$ . The boundary value  $f_0$  for  $f(s)$  is easily found to be

$$f_0 = 4(c_m^u - c_m^l)^{-2} \{ 1 - [1 - (s_0/2) (c_m^u - c_m^l)^2]^{1/2} \}.$$

At the outer rim of the cell we have the same conditions as for a cup-shaped cell. So we now have seven unknown boundary values  $s_0, c_m^u, c_m^l, c_m^m, f_m, \gamma, s_m$ . The matching conditions at two intermediate points in the intervals  $s_0 < s < s_m$  and  $s_m < s < 1 - s_0$  give us six equations. The seventh equation is obtained

from the condition of contact  $z(s_0) = z(1 - s_0)$ . The seven non-linear equations are solved by the Newton-Raphson method. We may view the codocyte I as an asymmetric torocyte. In analogy to the cup-shaped cell the codocyte I becomes more and more symmetric as we reduce the volume (or increase  $\Delta p$ ). In figure 18 the volume is plotted versus the pressure difference  $\Delta p$  for codocytes as well as for torocytes. As for the cup-shaped cell, we find a critical volume  $V_t$  below which no solution of codocyte I type exists.

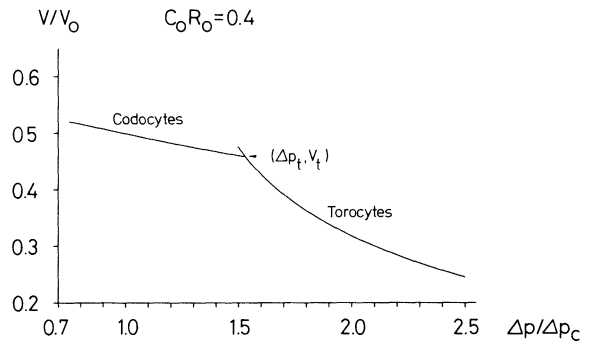


FIG. 18. — Plot of volume versus pressure difference for torocytes and codocytes I. The torocyte branch ends at a point slightly above the threshold  $V_t$  for codocyte I where it joins the discocyte branch not shown in this figure.

Let us now return to the deep cup-shaped cell of figure 16. If we reduce the pressure difference  $\Delta p$ , the volume increases slowly and the cell becomes more asymmetric. Finally the vesicle assumes a new type of shape, called stomatocyte, where the deep indentation in figure 16 becomes almost totally concave as shown in figure 19. The numerical calculations are rather difficult for these forms because the variable  $f(s)$  now has two maxima and one minimum as compared to only one maximum for the cup-shaped cell. The additional extrema in the function  $f(s)$  present two additional singularities which have

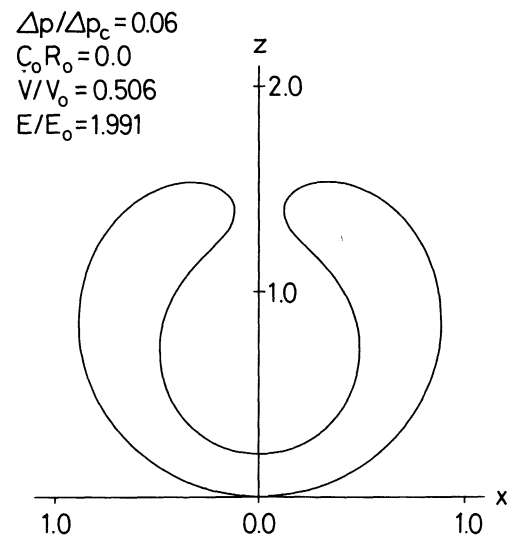


FIG. 19. — Contour of a stomatocyte.

to be removed in the same way as was outlined above for the cup-shaped cell. We have to divide the interval  $0 \leq s \leq 1$  into five parts and find the solutions  $c_m(s)$ ,  $c_p(s)$ ,  $f(s)$  in these five intervals. The matching conditions at the four intermediate points which separate the five parts of the interval  $0 \leq s \leq 1$  provide twelve non-linear equations. Figure 20 shows the volume  $V/V_0$  as a function of  $\Delta p/\Delta p_c$  for stomatocytes and for cup-shaped cells. We could not calculate the solutions in the range of  $\Delta p$  where the cell goes from the cup-shaped form to the stomatocyte shape, because higher order terms in the expansion (3.3) are required to obtain sufficient accuracy.

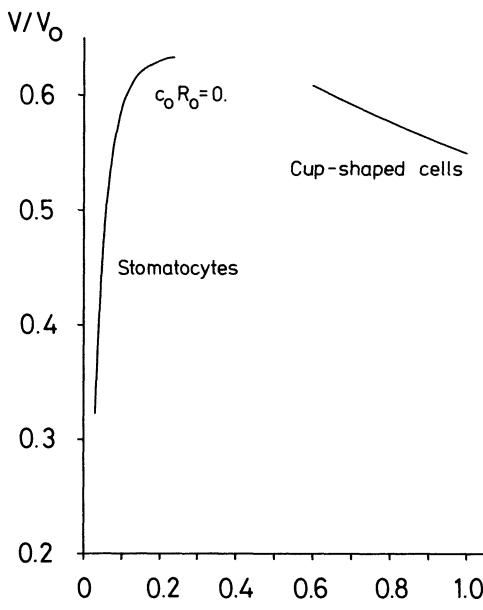


FIG. 20. — Plot of volume versus pressure difference for stomatocytes and cup-shaped cells.

For  $c_0 = 0$  the stomatocytes were found to have a slightly lower energy than cup-shaped cells of the same volume. For sufficiently negative values of  $c_0$  the volume of the stomatocytes is nearly  $V_0$  and increases with decreasing  $\Delta p$ . Figure 21 shows a stomatocyte for  $c_0 R_0 = -2.0$ .

If we make  $c_0$  sufficiently positive, the thickness at the center of the stomatocyte is reduced and we obtain contact as is shown in figure 22. This type of solution is called codocyte II. The boundary conditions at the circle bounding the area of contact are identical to those of codocyte I. The other boundary conditions are the same as for stomatocytes. As the volume of the codocyte II is reduced, the opening at the top becomes narrower and the area of contact increases (Fig. 23). Figure 24 gives volume  $V$  versus pressure-difference  $\Delta p$  for codocyte I and codocyte II, the curve being similar to the corresponding function for stomatocytes and cup-shaped cells as shown in figure 20.

**4. Concluding remarks.** — Many of the shapes calculated here have recently been observed experi-

$$\begin{aligned} \Delta p/\Delta p_c &= -0.85 & V/V_0 &= 0.9325 \\ C_0 R_0 &= -2.0 & E/E_0 &= 1.1362 \end{aligned}$$

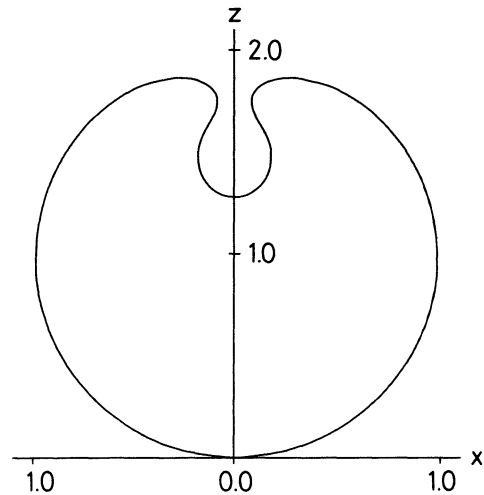


FIG. 21. — Contour of a nearly spherical stomatocyte.

$$\begin{aligned} \Delta p/\Delta p_c &= 0.26 \\ C_0 R_0 &= 0.60 \\ V/V_0 &= 0.339 \end{aligned}$$

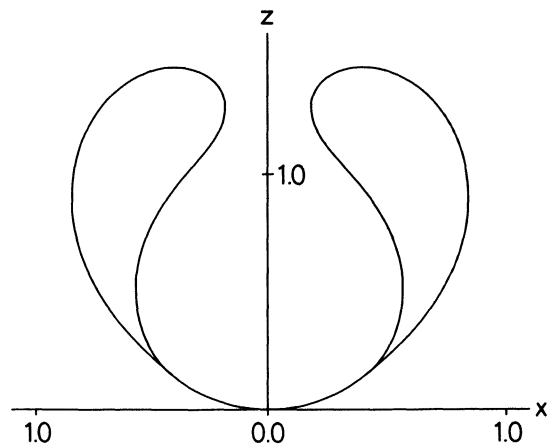


FIG. 22. — Contour of a codocyte II.

mentally [12, 13]. The vesicles were obtained by simple swelling of small pieces of lecithin in water. Some of them were quite large, having diameters between 10 and 30  $\mu$ .

Well-defined contours could be seen and photographed under a phase contrast microscope. The number of bilayers forming the membrane varied, but was apparently one in many cases. With the spontaneous curvature as the only adjustable parameter, theoretical shapes could be fitted very accurately to the experimental ones. These comparisons, which will be published elsewhere, leave no doubt

$$\begin{aligned}\Delta p/\Delta p_c &= 0.15 \\ C_0 R_0 &= 0.6 \\ V/V_0 &= 0.206\end{aligned}$$

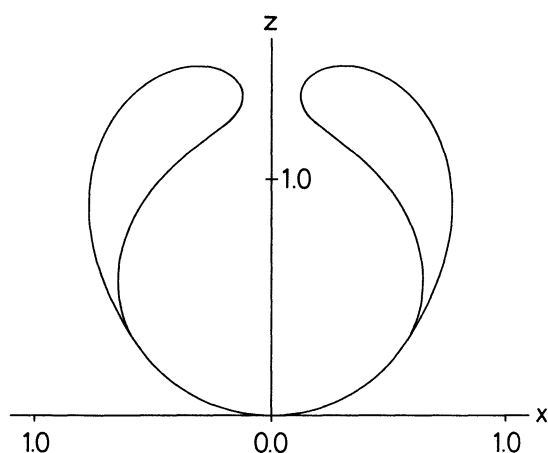


FIG. 23. — Contour of an almost closed codocyte II.

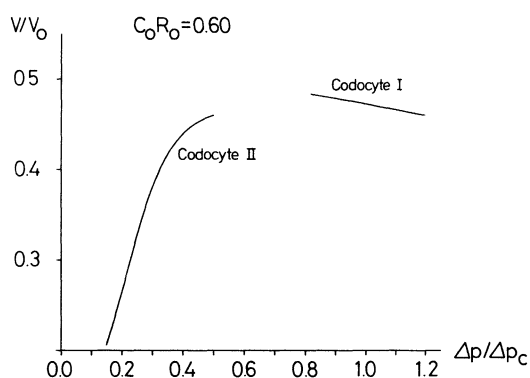


FIG. 24. — Plot of volume versus pressure difference for codocyte I and codocyte II.

that the shape of the closed membranes in their fluid state is controlled solely by curvature elasticity. They also confirm that the two halves of the membrane, where they are in contact, do not noticeably attract each other, as was assumed in the above calculations.

An important difference between vesicles and drops which is sometimes overlooked is the absence of surface tension in the former. A closed fluid membrane experiences virtually no tensile stress unless water is pumped into the enclosure, e.g. by osmosis, beyond the point where the spherical shape is reached. For smaller volumes, the membrane, whose area is practically constant, undergoes out-of-plane fluctuations. They do not destroy the equilibrium contour, but were found to be easily visible under the microscope if the membrane consists of only a small number of lecithin bilayers [12, 13]. In fact, they can be used to determine the value of the curvature-elastic modulus  $k_c$ . Theory [3, 4] and experiment [13] indicate the order of  $10^{-12}$  erg for  $k_c$ . Although the equilibrium

shape is governed by curvature elasticity, it gives no information on  $k_c$ . For large vesicles, the elastic modulus is too small by many powers of ten to affect significantly internal pressure and hence shape under given osmotic conditions. As an example, the critical pressure calculated from equation (B.4) with  $k_c = 10^{-12}$  erg and  $R_0 = 10 \mu$  is of the order of  $10^{-3}$  dyn  $\text{cm}^{-2}$ .

The curvature elasticity of fluid membranes can be used to explain certain red blood cell shapes [5, 7]. It may be important for some biological processes since it might govern the elastic behaviour of plasma membranes. Artificial vesicles and bilayer elasticity could also have other applications. From a fundamental point of view, vesicles seem to offer attractive possibilities for the study of phase transitions in two-dimensional systems. For instance, the fluid-solid transition of lecithin bilayers was seen under the phase contrast microscope [12] and some bilayer properties near the transition, which is probably close to second order, may be obtainable by more refined optical studies.

**Appendix A : Stability of the solutions presented in figures 1-3.** — To investigate the stability of the solutions we have to calculate the deformational energy of vesicles which have the same volume and surface area as the forms in figure 3 but differ slightly in shape. As is readily seen from figures 1-2 the function  $c_p(s)$  may be well represented by the first few terms of a Fourier series. We write

$$\begin{aligned}c_p(s) &= \alpha + \beta \sin(\pi s) + \varepsilon \cos(2\pi s) + \\ &+ \gamma \cos(\pi s) + \delta \sin(2\pi s)\end{aligned}\quad (\text{A.1})$$

with five coefficients still to be determined. For a symmetric solution  $\gamma$  and  $\delta$  are zero by definition. From expression (A.1) we easily find the value  $s_m$  at which  $c_p(s)$  has a maximum. For vesicles having rotational symmetry the curvatures  $c_m(s)$  and  $c_p(s)$  are connected with the variable  $f(s) = x^2$  by the following relations which have been derived in section 2

$$\frac{df}{ds} = \pm 4(1 - fc_p^2)^{1/2}\quad (\text{A.2})$$

$$\frac{dc_p}{ds} = \pm 2(1 - fc_p^2)^{1/2} (c_m - c_p)/f.\quad (\text{A.3})$$

We solve equation (A.2) for  $f(s)$  in the intervals  $0 \leq s \leq s_m$  and  $s_m \leq s \leq 1$  starting at  $s = s_m$  with the initial condition  $f(s_m) = [c_p(s_m)]^{-2}$ . The boundary conditions  $f(0) = 0$  and  $f(1) = 0$  along with the constraint

$$V/V_0 = (3/2) \int_0^1 f(s) c_p(s) ds = \text{const.}\quad (\text{A.4})$$

determine the coefficients  $\alpha$ ,  $\beta$  and  $\delta$ . We find the function  $c_m(s)$  from relation (A.3) which we rewrite as

$$c_m(s) = c_p(s) \pm (1/2) f(s) \times \\ \times (1 - f(s) c_p^2(s))^{-1/2} dc_p(s)/ds. \quad (\text{A.5})$$

We can now calculate the deformational energy

$$E/E_0 = \int_0^1 (c_m(s) + c_p(s) - c_0)^2 / (2 - c_0)^2 ds \quad (\text{A.6})$$

as a function of the coefficients  $\varepsilon$  and  $\gamma$  and find the minima of  $E$  with respect to  $\varepsilon$  and  $\gamma$ . The results obtained in this way agree well with the results shown in figures 1-3.

A simple way to tell from a  $V - \Delta p$  plot which of two shapes of equal volume has the lower elastic energy is to make use of the integral

$$\int_1^2 \Delta p dV$$

along the equilibrium curve connecting the shapes 1 and 2 which is just equal to the difference  $E_1 - E_2$  of the elastic energies. Consequently, the shape at smaller  $\Delta p$  has lower energy if the connecting curve goes through larger volumes. The shape at larger  $\Delta p$  is favoured if the path is through smaller volumes.

**Appendix B : Calculation of the critical spontaneous curvature.** — Here we give an outline of the calculation for the critical spontaneous curvature  $c_{0c}$  below which oblate ellipsoids are more stable than prolate ones for infinitesimal deformations.

We started from the balance of torque densities (per area) for rotationally symmetric forms,

$$(k_c/2) (c_p^2 - 2 c_p c_0 + c_0^2 - c_m^2) \sin \psi / \cos \psi + \\ + (\Delta p/2) x / \cos \psi \\ - k_c \cos \psi d(c_m + c_p)/dx = 0 \quad (\text{B.1})$$

which is equivalent to equation (2.1). For the sphere the tilt angle  $\psi$  of the membrane as a function of radius  $x$  is given by  $x = R_0 \sin \psi_{\text{sph}}$ . We then introduced an ellipsoidal deformation represented by the second Legendre polynomial

$$R - \tilde{R}_0 = s = (3/2) s_2 (\cos^2 \theta - 1/3) \quad (\text{B.2})$$

where  $\tilde{R}_0(s_2)$  is the renormalized sphere radius keeping the membrane area constant and  $\theta$  the polar angle. The associated change  $\Delta\psi$  as a function of  $x$  is

$$\Delta\psi = (3/2) s_2 \cos \psi_{\text{sph}} \sin \psi_{\text{sph}} \quad (\text{B.3})$$

where  $x = \tilde{R}_0 \sin \psi_{\text{sph}}$  relates  $x$  and  $\psi_{\text{sph}}$ . The curvatures  $c_m$  and  $c_p$  and their derivatives as well as  $\cos \psi$  and  $\sin \psi$  were expanded in powers of  $s_2/R_0$  up to second order, always using  $\sin \psi_{\text{sph}}$  and  $\cos \psi_{\text{sph}}$  instead of  $x$ .

The expansions were inserted in to (B.1) and the coefficients of equal powers were equated to zero. The equation for  $s_2$  recovers the critical pressure

$$\Delta p_c = (2 k_c / R_0^3) (6 - c_0 R_0) \quad (\text{B.4})$$

at which the sphere is in neutral equilibrium. The equation for  $s_2^2$  contains contributions which must be balanced by a deformation corresponding to the fourth Legendre polynomial. Upon separating them and inserting  $\Delta p_c$  in the remaining equation, one obtains  $c_{0c} R_0 = -39/23$  for the critical spontaneous curvature. The computation involves too many terms to be shown here.

Energetically the calculation amounts to a Landau expansion. Only terms quadratic and cubic in the order parameter  $s_2$  are considered. The critical spontaneous curvature makes the cubic term vanish. To lowest order, the amplitude  $s_4$  of the fourth Legendre polynomial is proportional to  $s_2^2$ . The associated energy varies as  $s_2^4$  and is thus irrelevant for the present purpose.

## References

- [1] SHEETZ, M. P. and CHAN, S. I., *Biochemistry* **11** (1972) 4573.
- [2] PAGANO, R. and THOMPSON, T. E., *J. Mol. Biol.* **38** (1968) 41.
- [3] HELFRICH, W., *Z. Naturforsch.* **28c** (1973) 693.
- [4] HELFRICH, W., *Z. Naturforsch.* **29c** (1974) 510.
- [5] HELFRICH, W. and DEULING, H. J., *J. Physique Colloq.* **36** (1975) C1-327.
- [6] EVANS, E. A. and FUNG, Y. C., *Microvasc. Res.* **4** (1972) 335.
- [7] DEULING, H. J. and HELFRICH, W., *Biophys. J.* **16** (1976).
- [8] BESSIS, M., in *Red Cell Shape*, Ed. M. Bessis. R. I. Weed and P. F. Leblond (Springer-Verlag, New York-Heidelberg-Berlin) 1973.
- [9] DE GENNES, P. G., *The Physics of Liquid Crystals* (Clarendon Press, Oxford) 1974.
- [10] FRANK, F. C., *Discuss. Faraday Soc.* **25** (1958) 19.
- [11] See i.e. HILDEBRAND, F. B., *Introduction to Numerical Analysis* (McGraw-Hill, New York) 1956.
- [12] HARBICH, W., SERVUSS, R. M. and HELFRICH, W., *Phys. Lett.* **57A** (1976) 294.
- [13] SERVUSS, R. M., HARBICH, W. and HELFRICH, W., *Biochim. Biophys. Acta* **436** (1976) 900.